

## Spontaneous Formation of Silica Nanoparticles in Basic Solutions of Small Tetraalkylammonium Cations

Joseph M. Fedeyko, Jeffrey D. Rimer, Raul F. Lobo,\* and Dionisios G. Vlachos\*

Center for Catalytic Science and Technology, Department of Chemical Engineering, University of Delaware, Newark, Delaware 19716

Received: June 2, 2004; In Final Form: July 1, 2004

We have found that the spontaneous formation of silica nanoparticles is a general phenomenon in basic solutions of small tetraalkylammonium (TAA) cations. The nanoparticle formation and structure have been investigated using conductivity, pH, and small-angle scattering methods. The particles have a core–shell structure with silica at the core and the TAA cations at the shell. The particle core size is nearly independent of the size of the TAA cation but decreases with pH, suggesting electrostatic forces are a key element controlling their size and stability. The nanoparticle formation is a reversible process at low temperatures, in several ways similar to surfactant aggregation into micelles. These silica nanoparticles may be a connection between the synthesis of zeolites and ordered mesoporous silicas such as MCM-41.

The chemistry of aqueous silica is complex and vital to the synthesis of important classes of materials<sup>1,2</sup> such as zeolites, used as industrial catalysts and sorbents. The chemistry of aqueous silica is also important in rock kinetics,<sup>3</sup> biomineralization,<sup>4</sup> soil sciences, and the biology of silica in plants.<sup>5,6</sup> Despite its long history, there remain important problems in silica chemistry requiring further understanding of the molecular processes that underpin many of the phenomena investigated in these areas. One of these problems is the role of silica nanoparticles formed in solutions of tetraalkylammonium (TAA) hydroxide and observed prior and during crystal growth of zeolites such as silicalite-1.<sup>7–11</sup>

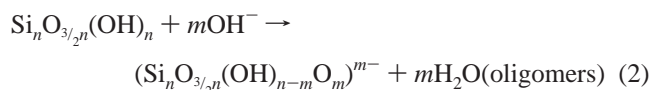
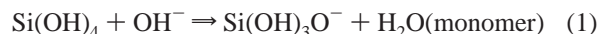
Here we report that the formation of silica nanoparticles is a rather general phenomenon that fulfills the three general characteristics of self-organized aggregates:<sup>12</sup> they form spontaneously, aggregation is a start–stop process (the addition of more silica results in more nanoparticles of the same size), and the aggregates have well-defined properties. These silica nanoparticles could play a unifying role in understanding a variety of processes and observations ranging from the synthesis of zeolites<sup>13,14</sup> and ordered-mesoporous silicas (OMS)<sup>15,16</sup> to the high solubility of silica in biological fluids.

We have found that silica–TAA hydroxide solutions have a well-defined critical aggregation concentration (CAC)—analogous to a critical micelle concentration<sup>12</sup>—below which silica is in the form of monomers and small oligomers,<sup>17</sup> and above which silica forms uniform nanoparticles in solution. Figure 1a shows the conductivity of solutions of tetrapropylammonium hydroxide (TPA OH) as a function of total silica concentration (added as tetraethyl orthosilicate, TEOS). Two clear regions are evident in the data: an initial region where the conductivity drops rapidly, and a second region after the CAC where the conductivity decreases slowly with silica concentration (see Table 1). A similar trend (Figure 1b) is observed following the pH, or hydroxide concentration (OH<sup>−</sup>), upon adding silica. The silica nanoparticles only form after the CAC (Figure 1c) as revealed by small-angle X-ray scattering (SAXS). Below the CAC the

SAXS pattern is essentially featureless, revealing the absence of any aggregates within the 1–40 nm length scale.<sup>18</sup> Above the CAC a clear increase in scattering is measured, demonstrating the appearance of silica nanoparticles. The nanoparticle formation is not due to condensation chemistry alone because this would lead to a broad distribution of particle sizes and a poorly defined CAC.<sup>19</sup> In this case the particles have a narrow size distribution and the CAC is sharp and well-defined.

Analysis of this SAXS pattern using the inverse Fourier transformation (IFT) method<sup>20</sup> leads to the pair-distance-distribution-function (PDDF) of Figure 1d. The PDDF indicates that these are individual particles having a maximum particle size of 4.5 nm at this specific composition. The shape of the experimental PDDF is also different from that of a sphere (Figure 1d, see below). The intensity of the SAXS patterns of solutions containing higher silica concentrations indicate that the number density of the nanoparticles increases, but their size remains nearly constant (Figure 1c). This behavior is also analogous to what is observed in surfactant aggregate systems as the surfactant concentration increases.<sup>21</sup>

The change in conductivity and pH below the CAC can be rationalized on the basis of the acid–base chemistry of silicic acid and silica oligomers. The conductivity drops because the consumption of the hydroxide anion by silicic acid exchanges a highly mobile anion (OH<sup>−</sup>) with larger, lower-mobility anions (Si(OH)<sub>3</sub>O<sup>−</sup> and its oligomers). The pH drops because of the acid–base reactions



where we have assumed, for simplicity, that silica oligomers are formed only of Q<sup>3</sup> species (Q<sup>n</sup> = SiO<sub>n</sub>(OH)<sub>4−n</sub>).<sup>22</sup>

Above the CAC, the pH remains nearly constant upon addition of relatively large quantities of silica (see Table 1). Above the CAC there is a change in the conductivity (Figure

\* Corresponding authors. R.F.L.: e-mail, lobo@che.udel.edu; phone, 302-831-1261. D.V.: e-mail, vlachos@che.udel.edu; phone, 302-831-8056.

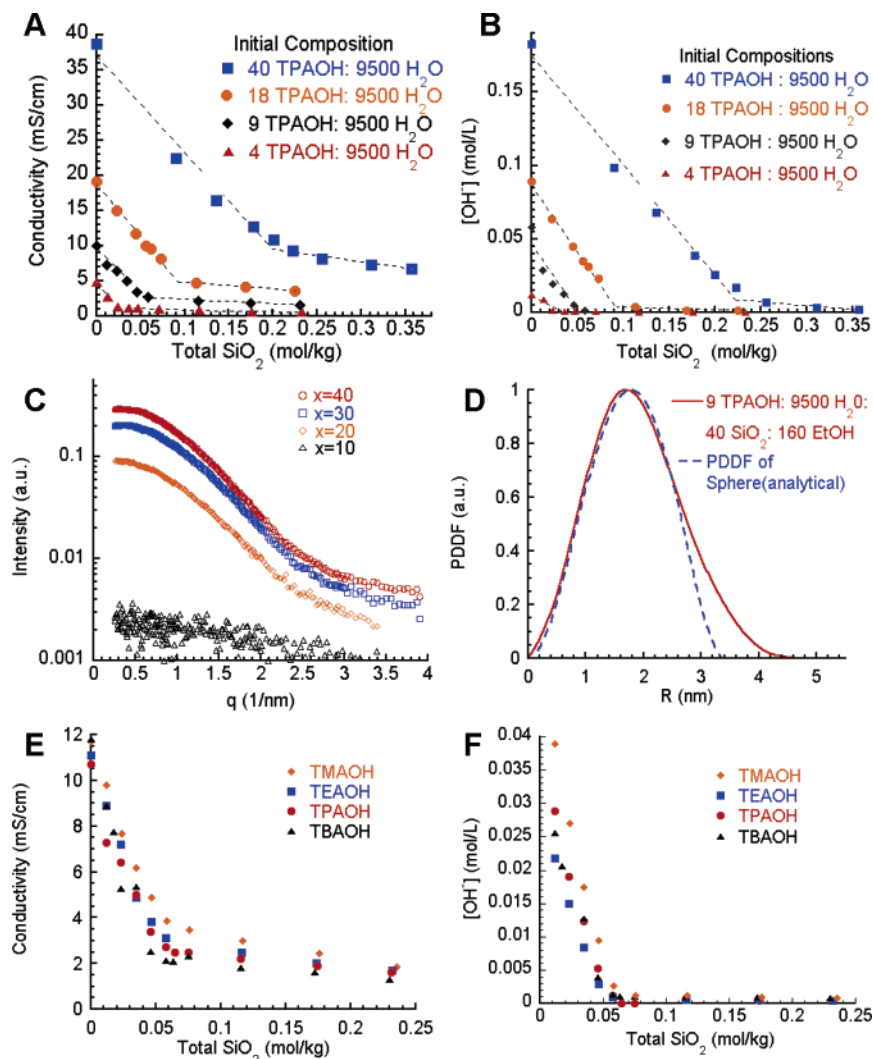


**Figure 1.** Determination of the critical aggregation concentration. (A) Conductivity as a function of total silica concentration for increasing amounts of initial TPAOH. The curves display a drastic change at the CAC, the point of a sudden change in slope, to higher silica concentrations at room temperature. The points are measurements, and the lines are linear fits. (B) Hydroxide concentration  $[\text{OH}^-]$  as a function of total silica in solution. The curves show the same trends observed with conductivity and the CACs determined by both methods coincide within experimental error. (C) SAXS patterns at different silica concentration ( $x$   $\text{SiO}_2$ :9 TPAOH:9500  $\text{H}_2\text{O}$ : $4x$  EtOH) but identical TPAOH concentration. After the CAC the particle concentration increases with increasing silica concentration. (D) Comparison of the PDDF of a sphere and the one from the SAXS patterns for  $x = 40$  indicates that the particles are not spherical. (E) Conductivity and (F) pH measurements for different TAA cations as a function of total silica concentration. Variations in the TAA cause almost no change in the location of the CAC for solutions with an initial base concentration of 9 TAAOH:9500  $\text{H}_2\text{O}$ .

**TABLE 1: Critical Aggregation Concentrations and Charge Density for Selected Initial Concentrations of TAAOH**

initial composition	critical aggregation concentration <sup>a</sup> ( $\text{SiO}_2$ eq, mol/kg)		$\Delta[\text{OH}^-]/\Delta[\text{SiO}_2]$		$\Delta S/\Delta[\text{SiO}_2]^b$ mS/cm (mol $\text{SiO}_2$ /kg)		$n:m^c$	$R_g^d$ nm
	from conductivity	from pH	below CAC	above CAC	below CAC	above CAC		
4.5 TPAOH:9500 $\text{H}_2\text{O}$	0.024	0.033	-0.36	-0.0015	-155	-3.53	14.7	2.0
9 TPAOH:9500 $\text{H}_2\text{O}$	0.054	0.056	-0.60	-0.0013	-133	-5.47	8.6	1.5
18 TPAOH:9500 $\text{H}_2\text{O}$	0.092	0.092	-0.90	-0.021	-150	-9.86	5.4	1.3
40 TPAOH:9500 $\text{H}_2\text{O}$	0.20	0.22	-0.75	-0.046	-139	-18.7	2.8	0.45
9 NaOH:9500 $\text{H}_2\text{O}$	0.047				-158	-8.5	9.3	1.84
9 TMAOH:9500 $\text{H}_2\text{O}$	0.052	0.058	-0.77	-0.0028	-147	-10.9	6.7	1.8
9 TEAOH:9500 $\text{H}_2\text{O}$	0.049	0.049	-0.55	-0.0029	-160	-7.97	7.8	1.5
9 TPAOH:9500 $\text{H}_2\text{O}$	0.054	0.056	-0.60	-0.0013	-133	-5.47	8.6	1.5
9 TBAOH:9500 $\text{H}_2\text{O}$	0.046	0.056	-0.55	-0.0015	-192	-5.15	9.4	1.6

<sup>a</sup> The equivalence points for the different solutions are: 0.026, 0.052, 0.103, and 0.223 mol/kg for the four TPAOH solutions, respectively. The equivalence point of the other solutions is  $\sim 0.052$  mol/kg. <sup>b</sup> Change in conductivity of the solution ( $\Delta S$ ) per mole of  $\text{SiO}_2$ . <sup>c</sup> This is calculated from the ratio of the conductivity at the CAC and the slope of the conductivity curve above the CAC. The conductivity at the CAC has been corrected for the small effect due to the concentration of TPAOH remaining in the solution. <sup>d</sup> Radius of gyration determined from the PDDFs following ref 20. The composition is constant and equal to 40  $\text{SiO}_2$ :Y TAAOH:9500  $\text{H}_2\text{O}$ :160 EtOH in the last five rows.

1a), but it is not as pronounced as before the CAC. This difference in slopes of conductivity and pH

the CAC shows that as the silica is added to the solution, dissolved silica is being sequestered from the aqueous phase

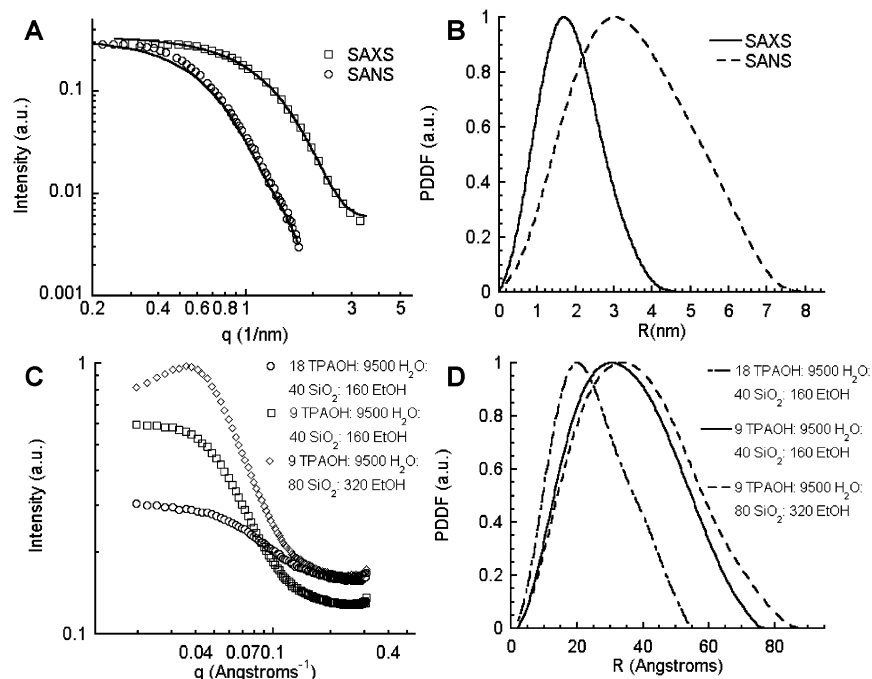
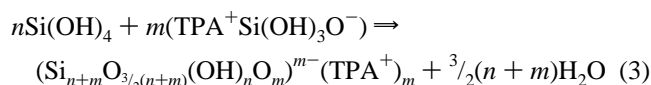


**Figure 2.** Nanoparticle structure and its dependence on pH and silica concentration. (A) Measurements of SANS and (B) SAXS patterns of a nanoparticle solution ( $x$  SiO<sub>2</sub>:9 TPAOH:9500 H<sub>2</sub>O:4x TEOS,  $x = 40$ ) reveal a clear difference in the particle size. The low electron density of the outer layer of these particles, which is primarily composed of TPA<sup>+</sup> cations, is similar to water and does not scatter X-rays effectively. This layer is not observed in the SAXS patterns and PDDF. (C) SAXS and (D) PDDFs of solutions of different composition. The size and shape of the nanoparticle change only slightly by doubling of the initial silica concentration. However, doubling the initial TAAOH concentration causes a significant decrease in the particle size.

and used as one of the building blocks of the nanoparticles; otherwise no further changes in conductivity would be observed. Taken together these observations indicate that the chemical transformations occurring above the CAC can be described by



Deconvolution of the liquid <sup>29</sup>Si NMR spectra of nanoparticle suspensions<sup>23</sup> (not shown) indicates that most of the silica is in the Q<sup>3</sup> form (typically ~75%) whereas the remainder is primarily Q<sup>2</sup>. The formation and dissolution of these nanoparticles is reversible as the particles dissolve upon reducing the silica concentration below the CAC with additional TPAOH aqueous solution in about 3 h.

The CACs calculated from conductivity and pH data are very similar (Table 1) and follow closely the equivalence point of the solution. The pH at the CAC increases as expected from the equivalence point of solution of a strong base (TPA OH) and a weak acid (Si(OH)<sub>4</sub>). Because the conductivity of the solutions at the CAC is dominated by contributions from TPA<sup>+</sup> and dissolved silica (Si(OH)<sub>3</sub>O<sup>-</sup> and its oligomers), it is possible to use the slope of the conductivity after the CAC to estimate a value for the ratio  $n:m$  of eq 3. Physically, this is the ratio of deprotonated silica units in the particles ( $\equiv\text{SiO}^-$ ) with respect to the number of neutral units ( $\equiv\text{SiOH}$ ). As the initial concentration of TPAOH increases, the ratio  $n:m$  decreases (Table 1); hence, the particles are more charged. At the same time, the particle size (from SAXS) also decreases as the initial concentration of TPAOH increases.

The spontaneous formation of silica nanoparticles is not limited to TPA<sup>+</sup> solutions. We have detected the formation of similar nanoparticles with other small TAA cations—tetramethylammonium (TMA), tetraethylammonium (TEA), and

tetrabutylammonium (TBA)—and sodium. We were surprised to find stable nanoparticles using NaOH solutions as it has been reported<sup>17</sup> that these precipitate soon after the equivalence point is crossed. The conductivity vs composition of these solutions follows closely the trends observed for TPA<sup>+</sup> and the pH vs composition curves virtually overlap the measurements of the TPAOH solutions (Figure 1e,f). We only find nanoparticles formed under basic conditions, although neutral and acid conditions were not investigated extensively.

We have used small angle neutron scattering (SANS) and SAXS to investigate the structure of the nanoparticles. In this system X-rays are scattered primarily by silica whereas neutrons are scattered by both silica and TAA cations. SANS and SAXS measurements at low concentrations of silica and TPA<sup>+</sup> (40 SiO<sub>2</sub>:9 TPAOH:9500 H<sub>2</sub>O:160 EtOH, about 1% vol) reveal that the nanoparticles have a core composed mostly of partially polymerized silicic acid surrounded by a shell composed of TPA<sup>+</sup> and water. This is evident from the SAXS and SANS scattering patterns (Figure 2a) and the corresponding PDDFs (Figure 2b). These measurements prove that the particles have a core-shell structure and also contain information about particle shape. Results of ongoing investigations of the SANS and SAXS patterns using a variety of particle shapes will be reported elsewhere.

The SAXS and SANS measurements (Figure 2c,d) indicate that the particles change little in size upon the addition of more silica to the solutions and that at constant silica concentration additional TPAOH leads to smaller particles. The stability of the particle size with increased silica concentration is an additional similarity between the properties of the TPA-silica system and surfactant aggregates. The reduction in particle size with TPAOH concentration is, on the other hand, probably the result of their core-shell structure. At higher pH, the fraction of charged silica units in the nanoparticle increases (Table 1) and as the surface charge density of the layer of cations on the

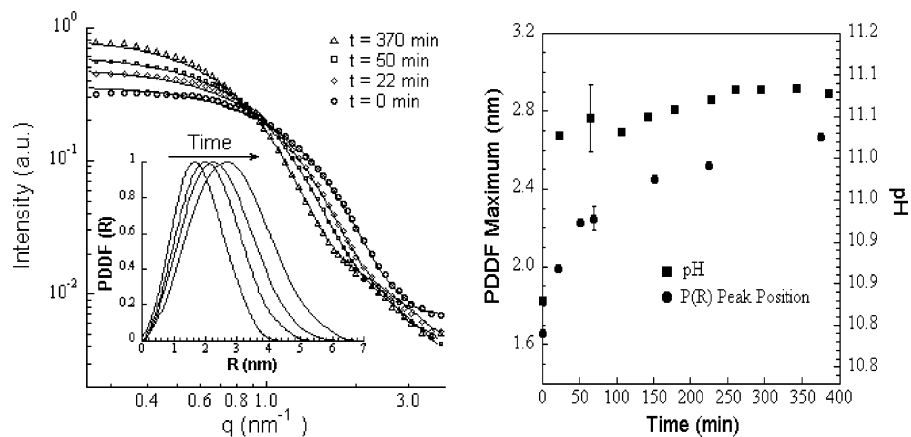


**Figure 3.** (a) SAXS patterns of silica nanoparticles measured at room temperature ( $t = 0$  min) and after heating at  $90^\circ\text{C}$  for 22, 50, and 370 min. The inset plots the PDDF curves obtained from IFT of the scattering data. The symbols are experimental measurements and the lines are the corresponding IFT fits. (b) Plots of the solution pH for the heated samples along with the peak heights of the corresponding PDDF curves. The pH was measured at  $25^\circ\text{C}$  after quenching the solution. The particles' silica core increases in size from approximately 4 to 7 nm.

surface remains constant, the particle volume should decrease to balance the charge.

Information about particle composition can be obtained through the particle's scattering length density (SLD) that was measured using SANS contrast-matching experiments. Five contrast points (different mixtures of  $\text{D}_2\text{O}$  and  $\text{H}_2\text{O}$  in the synthesis solution) were used to determine the match point, i.e., the composition where the particle scattering would be equal to zero. The measurements were conducted for particles prepared with TPA- $d_{28}$  and TPA- $h_{28}$  and the SDLs were found to be  $5.95 \times 10^{-6}$  and  $2.22 \times 10^{-6} \text{ \AA}^{-2}$ , respectively. These numbers differ from the coherent SLD calculated for silicalite-1 crystals—the zeolite formed from these solutions at higher temperatures—and indicate that the composition and structure of the nanoparticles is unlike the zeolite formed from these solutions ( $4.94 \times 10^{-6}$  and  $2.71 \times 10^{-6} \text{ \AA}^{-2}$  for silicalite-1 with occluded TPA- $d_{28}$  and TPA- $h_{28}$ , respectively).<sup>24</sup> The particles contain a larger ratio of TPA/ $\text{SiO}_2$  than the zeolite. Unfortunately, because we do not know the amount of water present in the organic shell and the water occluded in the inorganic core of the particles, it is not possible to use these data to determine the precise composition of the particles.

The room-temperature data indicate that the composition of the TPA-silica nanoparticles is different from the one of silicalite-1. This is at odds with reports by Watson and co-workers<sup>25</sup> and de Moor and co-workers<sup>11,26</sup> who found particles with composition close to the ZSM-5 zeolite. However, they heated the samples at  $90$ – $120^\circ\text{C}$  before conducting their measurements, and to resolve this disparity, we have followed the evolution of the nanoparticles after heating to  $90^\circ\text{C}$  for various periods of time (Figure 3a). The PDDFs of the SAXS patterns indicate that particles grow in size and change in morphology as the shape of the PDDF curves approaches the shape of a sphere. The changes in size (Figure 3b) correlate with the change of the solution pH with time, an indication of condensation of the silica core.

Besides their size and shape, the heated particles change in other ways compared to the room temperature particles. First, the particle suspensions do not reverse back to the low temperature dimensions for weeks. Furthermore, dilution of the nanoparticles with TPAOH at room temperature does not lead to rapid dissolution of the particles, as was observed above. This is likely a consequence of the condensation of the silica core at higher temperatures that in effect reduces the chemical potential of the silica in the nanoparticles. The difference

between previous observations<sup>11,25,26</sup> and ours indicate that the thermal history of the system is an important variable in understanding nanoparticle structure.

The results reported here greatly amplify the scope and complexity of the original ideas on silica nanoparticles described by Iler.<sup>1</sup> The nanoparticles are not only stable in a fully condensed form, as he suspected, but span a range of sizes and levels of internal connectivity. We have shown that these nanoparticles can be easily prepared using symmetric small TAA cations, but many other organic cations are likely to show similar or related behavior. The low-temperature reversibility of the nanoparticles is a significant observation as it allows for the application of self-assembly equilibrium theories to these systems.

The results presented here also indicate that many of the interactions leading to the formation of TAA-silica nanoparticles are similar to the interactions that lead to the formation of ordered-mesoporous-silicates (such as MCM-41) with one important difference. In the synthesis of OMS, the organic TAA cations—such as cetyltrimethylammonium—self-assemble alone due to attractive hydrophobic forces between molecules. Small TAA cations such as the ones investigated here do not associate in aqueous solutions.<sup>27</sup> In the absence of attractive hydrophobic interactions, the force between particles is repulsive, which explains their stability in aqueous solutions. We believe that the study of the silica nanoparticles reported here could lead to insights into OMS, just as the study of micelles has been central to understanding more complex surfactant structures.<sup>19</sup> The fact that essentially identical particles are obtained for cations as different as  $\text{TMA}^+$  and  $\text{TBA}^+$  suggests that electrostatic forces play a predominant role in controlling particle size and structure.

It is possible that the stabilization of silica by organic molecules<sup>6,28</sup> to form nanoparticles is a phenomenon that has been so far overlooked in other areas. Silica nanoparticles may be relevant in biomineralization<sup>29–31</sup> where it has been argued that stable inorganic nanoparticles could be important in the growth of crystals in living organisms. Water-rock kinetics in geosciences<sup>32</sup> is important to the study of global change, the role of fluids in the earth, and environmental concerns,<sup>33</sup> and organic-silica nanoparticles may be among the variables that govern the rates and mechanisms of the interaction between rocks and fluids in locations where the organic content of the fluid is large.<sup>4</sup> To the best of our knowledge, organic-stabilized silica nanoparticles have not been considered and may well

explain long-standing puzzles in silicon biogeochemistry such as the persistence of silica in biological fluids.

## Materials and Methods

**Synthesis.** Solutions of varying silica and TAA concentrations were synthesized by first diluting concentrated TAA aqueous solutions (TMAOH, 25% w/w, TEOH, 35% w/w and TPAOH, 40% w/w from Alfa Aesar, TBAOH, 40% w/w aqueous, Aldrich) in deionized water. After mixing for ~30 min, TEOS (98%, Aldrich) was added and the resulting mixture was vigorously stirred for at least 12 h prior to analysis. To investigate the effect of temperature on the nanoparticles, the samples were placed in polypropylene tubes and submerged in a water bath regulated at 90 °C. Individual samples were removed at various times and cooled to room temperature before measurement. The conductivity measurements were obtained with a VWR Model 2052 EC Meter and the pH was measured using a Corning 355 pH/ion analyzer and a Corning high-performance electrode with Ag-ion barrier. The pH meter was calibrated with standardized pH 10 and 12 buffer solutions (Alfa Aesar). CAC points were determined using solutions of composition  $X \text{ SiO}_2:Y \text{ TPAOH}:9500 \text{ H}_2\text{O}:4X \text{ EtOH}$  where  $X = 0-40$  and  $Y = 4.5-40$ . The solution used for SANS and SAXS measurements was of composition  $40 \text{ SiO}_2:9 \text{ TPAOH}:9500 \text{ H}_2\text{O}:160 \text{ EtOH}$  (referred to as C4) unless otherwise noted. The same compositions were used for measuring the CAC of solutions with TMA, TEA, and TBA. Additional SANS measurements were performed with increased TPAOH ( $Y = 18$ ) and silica concentrations ( $X = 80, Y = 9$ ).

**Analytical Details.** SANS measurements were conducted on the 30 m instrument (NG3) at the National Institute of Standards and Technology at Gaithersburg, MD. Samples were prepared following the above methods with  $\text{D}_2\text{O}$  replacing water to increase the contrast between the background and the nanoparticles. The samples were placed in quartz cells of 4-mm path length. A constant neutron wavelength of 6 Å was used with a 2.2 m sample-to-detector distance. Software provided by NIST was used for the normalization of the data and the subtraction of the scattering from the sample holder. Small-angle X-ray scattering experiments were conducted on a SAXSess (Anton-Parr), small-angle X-ray scattering system. Samples were placed in a vacuum-tight 1 mm diameter quartz capillary holder, and measured at 25 °C. Cu K $\alpha$  radiation ( $\lambda = 1.54 \text{ \AA}$ ) was used with a 265 mm sample-to-detector distance. The scattering patterns were collected on a phosphor imaging plate with in the  $q$  range  $0.077-8 \text{ nm}^{-1}$ . Patterns are normalized to the height of the primary beam signal using the SAXSquant software. Desmearing was conducted by subtracting the signal from a normalized deionized water sample. Both SAXS and SANS patterns were further analyzed using the Generalized Indirect Fourier Transform (GIFT) version 5-2000 software. The subtracted scattering patterns were fit with a form factor followed by indirect Fourier transform to obtain pair distance distribution functions.

**Acknowledgment.** We acknowledge K. Sawant (U. Del) for her help collecting the  $^{29}\text{Si}$  NMR spectra. The X-ray experiments were made with a SAXSess small-angle X-ray instrument on loan from Anton Paar GmbH, in Graz/Austria. We acknowledge the support of the National Institute of Standards and Technology, U.S. Department of Commerce, in providing the neutron research facilities used in this work. This report is based on work funded by the National Science Foundation under Grant No. 0103010.

**Supporting Information Available:** Solution  $^{29}\text{Si}$  NMR spectra. This material is available free of charge via the Internet at <http://pubs.acs.org>.

## References and Notes

- (1) Iler, R. K. *The Chemistry of Silica: solubility, polymerization, colloid and surface properties and biochemistry*; Wiley: New York, 1979.
- (2) Brinker, C. J.; Scherer, G. W. *Sol-gel science: the physics and chemistry of sol-gel processing*; Academic Press: San Diego, 1990.
- (3) Dove, P. M. *Geochim. Cosmochim. Acta* **1999**, *63*, 3715.
- (4) Kubicki, J. D.; Heaney, P. J. *Geochim. Cosmochim. Acta* **2003**, *67*, 4113.
- (5) Richmond, K. E.; Sussman, M. *Curr. Opin. Plant Biol.* **2003**, *6*, 268.
- (6) Kinrade, S. D.; Del Nin, J. W.; Schach, A. S.; Sloan, T. A.; Wilson, K. L.; Knight, C. T. G. *Science* **1999**, *285*, 1542.
- (7) Schoeman, B. J.; Regev, O. *Zeolites* **1996**, *17*, 447.
- (8) Kirschhock, C. E. A.; Buschmann, V.; Kremer, S.; Ravishankar, R.; Houssin, C. J. Y.; Mojet, B. L.; van Santen, R. A.; Grobet, P. J.; Jacobs, P. A.; Martens, J. A. *Angew. Chem., Int. Ed.* **2001**, *40*, 2637.
- (9) Kirschhock, C. E. A.; Kremer, S. P. B.; Grobet, P. J.; Jacobs, P. A.; Martens, J. A. *J. Phys. Chem. B* **2002**, *106*, 4897.
- (10) Nikolakis, V.; Kokkoli, E.; Tirrell, M.; Tsapatsis, M.; Vlachos, D. G. *Chem. Mater.* **2000**, *12*, 845.
- (11) de Moor, P.; Beelen, T. P. M.; Komanschek, B. U.; Diat, O.; van Santen, R. A. *J. Phys. Chem. B* **1997**, *101*, 11077.
- (12) Evans, D. F.; Wennerstrom, H. *The Colloidal Domain*, 2nd ed.; Wiley-VCH: New York, 1999.
- (13) de Moor, P. P. E. A.; Beelen, T. P. M.; van Santen, R. A. *Microporous Mater.* **1997**, *9*, 117.
- (14) Davis, M. E.; Lobo, R. F. *Chem. Mater.* **1992**, *4*, 756.
- (15) Bagshaw, S. A.; Prouzet, E.; Pinnavaia, T. J. *Science* **1995**, *269*, 1242.
- (16) Huo, Q. S.; Margolese, D. I.; Ciesla, U.; Feng, P. Y.; Gier, T. E.; Sieger, P.; Leon, R.; Petroff, P. M.; Schuth, F.; Stucky, G. D. *Nature* **1994**, *368*, 317.
- (17) Kinrade, S. D.; Knight, C. T. G.; Pole, D. L.; Syvitski, R. T. *Inorg. Chem.* **1998**, *37*, 4272.
- (18) Dynamic Light Scattering (DLS) of these solutions indicates the absence of particles with diameters within 10–1000 nm.
- (19) Hiemenz, P. C.; Rajagopalan, R. *Principles of Colloid and Surface Chemistry*, 3rd ed.; Marcel-Dekker: New York, 1997.
- (20) Glatter, O. *J. Appl. Crystallogr.* **1979**, *12*, 166.
- (21) Israelashvili, J. N. *Intermolecular and Surface Forces*, 2nd ed.; Academic Press: London, 1992.
- (22) The slope in Figure 1b is not 1 because the  $\text{pK}_a$  of silanols in the oligomers increases as the unit is progressively deprotonated.
- (23) The  $^{29}\text{Si}$  NMR spectra were acquired on solutions containing higher silica concentrations than the ones reported in Table 1. The low natural abundance, long relaxation times (over 100 s) and low concentration of silica in the samples made the acquisition time exceedingly long (more than 72 h) in the dilute samples. A typical composition for the NMR measurements was  $25 \text{ SiO}_2:9 \text{ TPAOH}:150 \text{ H}_2\text{O}:290 \text{ D}_2\text{O}:100 \text{ EtOH}$ , which is about 10 times more concentrated than the composition used for the SANS experiments. The fractions of  $\text{Q}^3$  and  $\text{Q}^2$  change depending on composition, but in general, we find a very small fraction of  $\text{Q}^1$  and  $\text{Q}^4$  groups in the nanoparticles, if any.
- (24) Watson, J. N.; Iton, L. E.; Keir, R. I.; Thomas, J. C.; Dowling, T. L.; White, J. W. *J. Phys. Chem. B* **1997**, *101*, 10094.
- (25) Watson, J. N.; Brown, A. S.; Iton, L. E.; White, J. W. *J. Chem. Soc., Faraday Trans.* **1998**, *94*, 2181.
- (26) de Moor, P.; Beelen, T. P. M.; Komanschek, B. U.; van Santen, R. A. *Micropor. Mesopor. Mater.* **1998**, *21*, 263.
- (27) Claesson, P.; Horn, R. G.; Pashley, R. M. *J. Colloid Interface Sci.* **1984**, *100*, 250.
- (28) Kinrade, S. D.; Hamilton, R. J.; Schach, A. S.; Knight, C. T. G. *J. Chem. Soc., Dalton Trans.* **2001**, 961.
- (29) Mann, S. *Nature* **1988**, *332*, 119.
- (30) Vrieling, E. G.; Beelen, T. P. M.; van Santen, R. A.; Gieskes, W. W. C. *J. Biotechnol.* **1999**, *70*, 39.
- (31) Colfen, H.; Mann, S. *Angew. Chem., Int. Ed.* **2003**, *42*, 2350.
- (32) Dove, P. M.; Rimstidt, J. D. Silica-Water Interactions. In *Silica: Physical Behavior, Geochemistry and Materials Applications*; Heaney, P. J., Prewitt, C. T., Gibbs, G. V., Eds.; Mineralogical Society of America: Washington, D.C., 1994; Vol. 29, p 259.
- (33) Bennett, P. C. *Geochim. Cosmochim. Acta* **1991**, *55*, 1781.